Chem. Ber. **116**, 2972 – 2982 (1983)

The Electronic Structure of Phosphorus Cages with the Nortricyclane Skeleton. – Model Calculations and Photoelectron Spectroscopic Investigations

*Rolf Gleiter**[a], *Michael C. Böhm*[a], *Mirjana Eckert-Maksić*[a,b], *Wolfgang Schäfer*[a], *Marianne Baudler*[c], *Yusuf Aktalay*[c], *Gerhard Fritz*[d], and *Klaus-Dieter Hoppe*[d]

Institut für Organische Chemie der Universität Heidelberg[a], Im Neuenheimer Feld 270, D-6900 Heidelberg,

Department of Organic Chemistry and Biochemistry, „Ruder Boscovič" Institute[b], Zagreb, Yugoslavia,

Institut für Anorganische Chemie der Universität Köln[c], D-5000 Köln, and

Institut für Anorganische Chemie der Universität Karlsruhe[d], D-7500 Karlsruhe

Received December 27, 1982

The different reactivity of $P_4[Si(CH_3)_2]_3$ (**1**) and $P_7(CH_3)_3$ (**2**) is discussed in terms of a simple MO scheme. This scheme is based on semiempirical calculations (MINDO/3, MNDO) and on He(I) photoelectron spectroscopic investigations on **1** and **2**. The electronic structure of similar cage compounds with the nortricyclane skeleton like P_7^{3-}, P_4S_3, and $P_7[Si(CH_3)_3]_3$ is compared with **1** and **2**.

Die Elektronenstruktur von Phosphor-Verbindungen mit Nortricyclan-Struktur. – Modell-Rechnungen und Photoelektronenspektren

Die unterschiedliche Reaktivität der Phosphor-Verbindungen $P_4[Si(CH_3)_2]_3$ (**1**) und $P_7(CH_3)_3$ (**2**) wird anhand eines einfachen MO-Schemas diskutiert. Das MO-Schema basiert auf semiempirischen Rechnungen (MINDO/3, MNDO) und auf He(I)-photoelektronenspektroskopischen Untersuchungen an **1** und **2**. Die Elektronenstruktur ähnlich gebauter Käfigverbindungen mit Nortricyclangerüst wie P_7^{3-}, P_4S_3 und $P_7[Si(CH_3)_3]_3$ wird mit **1** und **2** verglichen.

The phosphorus compounds $P_4[Si(CH_3)_2]_3$ (**1**)[1] and $P_7(CH_3)_3$ (**2**)[2] have been recently prepared and their structures have been determined by X-ray[3] and NMR studies[4]. Both compounds show the nortricyclane skeleton and therefore one should expect similar donor properties at the basal and apical P centers.

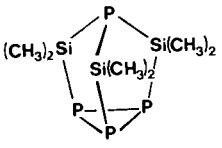

1

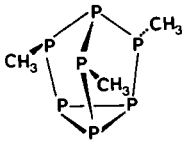

2a

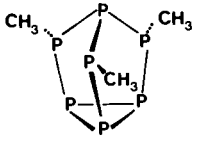

2b

0009 – 2940/83/0808 – 2972 $ 02.50/0

Recent investigations, however, indicate a marked difference between both compounds with respect to their capabilities to form transition metal carbonyl complexes. While **1** reacts with $Cr(CO)_6$ to yield $P_4(SiMe_2)_3Cr(CO)_5$ (**3**) and $[P_4(SiMe_2)_3Cr(CO)_4]_2$ (**4**)[4] readily, it is much more difficult to obtain $P_7(CH_3)_3Cr(CO)_5$ (**5**) from **2**[5] and so far $P_7[Si(CH_3)_3]_3$ (**6**) seems not to react at all[5].

$P_4(SiMe_2)_3Cr(CO)_5$	$[P_4(SiMe_2)_3Cr(CO)_4]_2$	$P_7(CH_3)_3Cr(CO)_5$	$P_7[Si(CH_3)_3]_3$
3	**4**	**5**	**6**

X-ray investigations on the two complexes **3** and **4** reveal that the transition metal is bound to one or two P atoms of the three-membered ring[6]. At first sight it is not obvious at all why **2** with the same P_3 unit is much less reactive under similar reaction conditions. To provide a basis of assessing the difference in reactivity between **1** and **2** we have carried out quantum-chemical model calculations on both compounds and have recorded their He(I) photoelectron (PE) spectra. As quantum-chemical methods we chose the MNDO[7] and MINDO/3[8] model since our recent investigations on P_7^{3-} [11] and $P_3(tBu)_3$ [12] have indicated that both semiempirical methods are capable to reproduce the electronic structure of small phosphorus rings with sufficient accuracy.

Bonding Model for 1 and 2

The geometrical parameters of **1** and **2** have been optimized with respect to the minimum of the total energy. In the case of **1** the results were close to the X-ray data reported[3]. For **2** we have carried out our calculations for both possible isomers **2a** and **2b** present in solution[2]. It turned out that the difference in energy and in the sequence of the MO's is very small (ΔH_f (**2a**) = 78.04 kJ/mol, ΔH_f (**2b**) = 80.10 kJ/mol according to MINDO/3) and therefore we assumed in most cases the configuration of higher (C_3) symmetry (**2a**). In Fig. 1 the calculated net charges (MNDO) at the P and Si atoms of **1** and **2** are indicated. A marked difference is predicted in so far as in the case of **1** all P atoms show a surplus of negative charge while in **2** only the equatorial P atoms are negatively charged. This difference in the net charges can be traced back to a considerable difference in the sequence of the highest occupied molecular orbitals, as well as to the localization properties of these MO's.

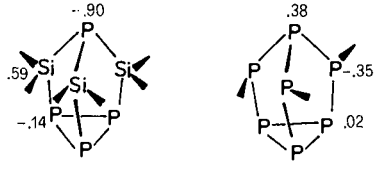

Fig. 1. Calculated (MNDO) net charges of $P_4[Si(CH_3)_2]_3$(**1**) and $P_7(CH_3)_3$ (**2**)

The highest occupied molecular orbitals of **1** and **2** can be composed approximately from the highest occupied MO's of the basal three-membered ring unit, the lone pair of the apical P atom and the highest occupied MO's of the equatorial centers. In Fig. 2 these orbitals of the three fragments are shown in a qualitative interaction diagram.

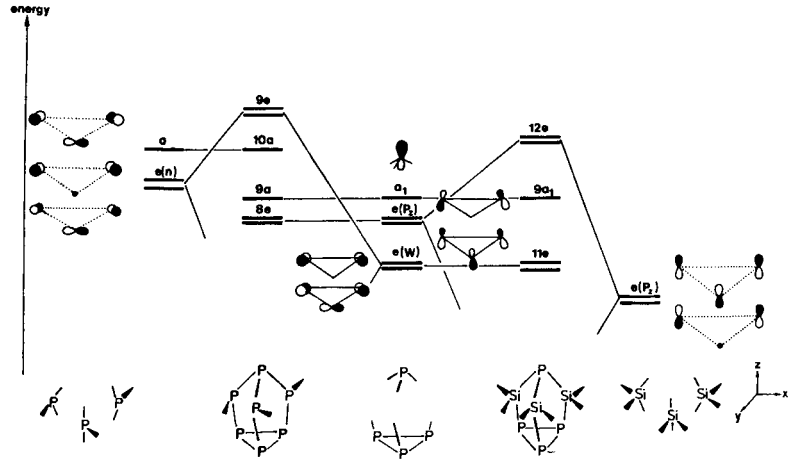

Fig. 2. Qualitative interaction diagram between a P_3 unit and a P atom (middle), a $(CH_3P)_3$ unit (left) and a $[Si(CH_3)_2]_3$ unit (right) to yield the highest occupied orbitals of **1** and **2**

On the left side of this diagram the three (e(n), a(n)) linear combinations of the 3p orbitals on three PCH_3 fragments in the *xy* plane are shown. In the center of Fig. 2 we have drawn the lone pair provided by the apical P atom (a_1) and two degenerate linear combinations located at the basal P_3 fragment, i.e. lone pair-combinations nearly parallel to the p_z axis ($e(p_z)$) and the Walsh type orbitals (e(W)). Recent investigations on three-membered phosphorus rings[12] have provided strong evidence that the lone pair and Walsh type MO's are close in energy as indicated in the diagram. On the right side of Fig. 2 we show a degenerate pair of orbitals ($e(p_z)$) localized at the $Si(CH_3)_2$ groups. Due to the different energy and symmetry of the orbitals provided by the fragments, a different interaction pattern results. In the case of **1** the lone pairs ($e(p_z)$) of the P_3 fragment interact strongly with the $(Si(CH_3)_2)_3$ fragment and thus the highest degenerate linear combination (12e) is mainly localized at the P_3 unit of **1**.

In the case of **2** the Walsh type linear combination of the basal P_3 unit interacts with the lone pair combination (e(n)) of the equatorial $(PCH_3)_3$ unit. This yields a HOMO (9e) which is mainly localized at the equatorial PCH_3 centers.

The qualitative interaction scheme presented in Fig. 2 is fully confirmed by semiempirical calculations. In Fig. 3 the contour diagrams of the highest occupied MO's of **1** and **2** as derived from MNDO calculations are shown. The section of the wave function belonging to 12e of **1** shows that the frontier electron density is concentrated below the P_3 ring while $9a_1$ is mainly located at the apical P atom. In the case of **2**, however, the HOMO (9e) is strongly localized at the equatorial P atoms ("lone pairs"). (The 9a orbital of **2** on the other hand is similar to the $9a_1$ combination of **1**.)

In Fig. 3 we also show contour plots of high lying orbitals which follow in energy those just discussed. In the case of **1** the 11e orbitals can be considered as a linear combination out of Walsh type orbitals localized in the three-membered ring while the 8e linear combinations of **2** show its maximum amplitude below the basal P_3 unit. In

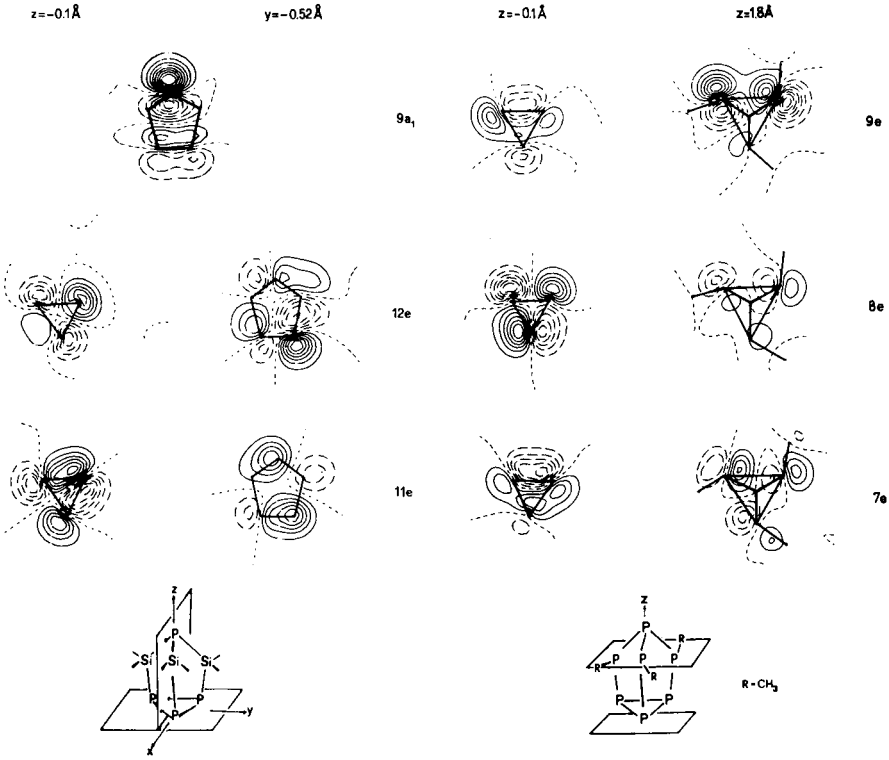

Fig. 3. Wave function contour diagrams of the highest occupied MO's of **1** and **2** according to a MNDO calculation

Table 1. Energy, symmetry, and contributions of the various AO's to the molecular orbitals of **1** and **2a** according to the MNDO method. The contributions to the MO's from the methyl groups are not displayed

Compound	ε_j(eV)	Γ_j	% P_b	% P_e	% Si	% P_a
1	− 9.80	$9a_1$	26.8		4.1	68.6
	− 9.82	12e	60.5		21.6	9.7
	−11.25	11e	33.8		15.7	11.0
	−11.53	10e	36.5		17.3	17.5
2a	−10.24	9e	25.7	63.6		3.6
	−10.78	10a	16.9	51.0		24.7
	−11.46	8e	68.8	20.1		6.4
	−11.52	9a	38.6	37.6		14.2
	−12.89	7e	34.3	33.1		7.4

addition to the simple picture provided by the qualitative interaction diagram in Fig. 2 the MNDO calculation predicts for **1** the sequence $9a_1$ on top of 12e with only a marginal difference, followed by 11e and 10e (see Table 1). The decomposition of the different molecular orbitals into atomic contributions is given in Table 1. Also those

orbitals are listed which are not shown in Fig. 3. The different reactivity of **1** and **2** towards $Cr(CO)_6$ can be understood by the different shape of the highest occupied molecular orbitals. In the case of **1**, an electrophile is predicted to attack at the basal and at the apical P atom. For **2**, however, the calculations predict a preference of the equatorial and apical P atoms. Thus we expect for **2** that a small electrophile attacks the equatorial positions while a sterically more ambitious electrophile might end up at

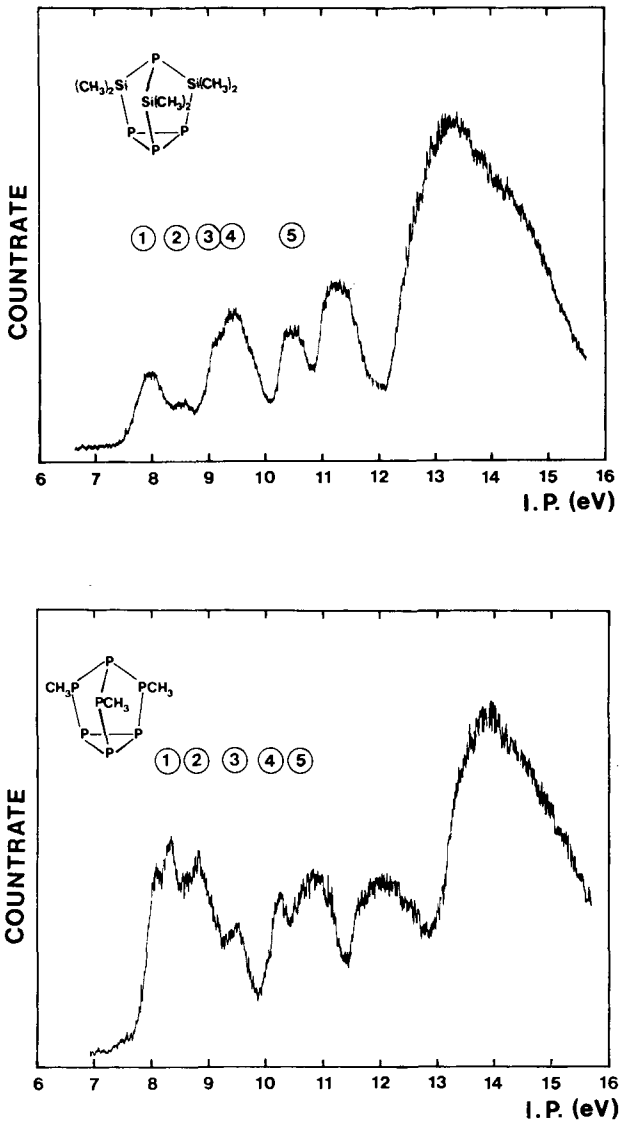

Fig. 4. He(I) PE spectra of **1** and **2**

the apical P atom. As a corollary from the different shape of the HOMO steric effects are expected to be more important in **2** and **6** than in **1**.

PE Spectroscopic Investigations

To find out whether the model calculations carried out on **1** and **2** are reliable we have investigated their He(I) photoelectron (PE) spectra which are shown in Fig. 4. Between 7.5 and 10 eV both spectra show a relatively large difference: In **1** we find two small bands in front of a broad one while in **2** a broad band is registered in front of a small one. To assign the number of transitions hidden in the first broad peak of **2** we have deconvoluted this band by assuming that the peak at 9.5 eV corresponds to a single ionization event and that the cross-sections of the other electron ejections are similar. This leads to the prediction that the first broad band in the PE spectrum of **2** is due to the superposition of five ionization events (see Fig. 5). In the case of **1** a similar deconvolution shows that the broad peak between 9 and 10 eV is due to four transitions.

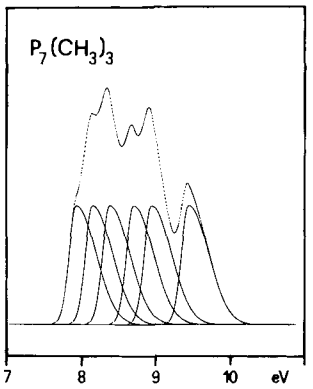

Fig. 5. Deconvolution of the first part of the PE spectrum of **2** assuming Gaussian type bands

To assign the first cationic states of **1** and **2** we assume the validity of Koopmans' theorem ($I_{v,j} = -\varepsilon_j$)[13], i.e. the measured vertical ionization potentials, $I_{v,j}$, are approximated by the calculated orbital energies, ε_j, for the ground state. This assumption implies small and about equal energy defects caused by electron correlation and relaxation during the ionization. To derive the orbital energies we make use of the MINDO/3 model[8,9] with modified P, C parameters[10] and the MNDO method[7].

In Table 2 we have compared the calculated orbital energies with the measured vertical ionization potentials of **1** and **2**. In the case of **2** we have only listed the results of a calculation on **2a** since the difference in the orbital energies between **2a** and **2b** is smaller than 0.2 eV. To match the bands obtained from our deconvolution with the calculated orbital energies we assume for **1** the sequence 12e above $9a_1$ followed by at least four closely spaced transitions arising from ionizations from 11e and 10e (see also Fig. 3 and Table 1).

Table 2. Comparison of the measured vertical ionization potentials $I_{v,j}$ of **1** and **2** with calculated ones for **2a** assuming the validity of Koopmans' theorem (w = Walsh-type combination)

Compound	Band	$I_{v,j}$	Assignment	$-\varepsilon_j$(eV) MNDO	$-\varepsilon_j$(eV) MINDO/3
1	①	8.0	n_P (ap)	9.80 ($9a_1$)	
	②	8.5	n_P (b)	9.82 (12e)	
	③	9.1	w (b)	11.25 (11e)	
	④	9.4	PSi-σ	11.53 (10e)	
	⑤	10.5	SiC-σ	11.84 ($4a_2$)	
			n_P (b)	12.08 ($8a_1$)	
2	①	8.3	n_P (eq)	10.24 (9e)	7.81 (9e)
	②	8.8	n_P (eq)	10.78 (10a)	8.15 (10a)
			n_P (b)	11.46 (8e)	8.82 (8e)
	③	9.5	n_P(ap)	11.57 (9a)	8.62 (9a)
	④	10.2	PP-σ	13.08 (8a)	10.16 (8a)
	⑤	10.8	w (b)	12.90 (7e)	10.27 (7e)
			PC-σ	14.20 (6e)	11.79 (6e)

In the case of **2** the orbital sequence 9e, 10a, 8e and 9a is assumed. The corresponding wave functions have been discussed in the previous section (see Fig. 3, Table 1).

The comparison between experiment and model calculation given in Table 2 shows that the used methods reproduce the sequence of the MO's satisfactorily.

PE Spectrum of 7

In addition to the PE spectra of **1** and **2** we also investigated that of the bicyclic compound $P_6(t\,Bu)_4$ (**7**) which has been prepared recently[14]. In Fig. 6 the PE spectrum

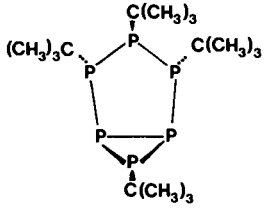

7

$P_6(CH_3)_4$ **8** P_7^{3-} **9** P_4S_3 **10** $P_7(SiH_3)_3$ **11**

is shown. To interprete the PE spectrum we have carried out MINDO/3 and MNDO calculations on $P_6(CH_3)_4$ (**8**) with the same conformation for the methyl groups as for the *tert*-butyl groups in the case of **7**. In Table 3 the first ionization potentials are compared with orbital energies. There is a good agreement between PE spectrum and MO calculation if we assume for the first peak (bands ① and ②) three, for the second one and for the third (bands ④ and ⑤) five ionization events. This assumption is in line with the intensity ratio of 2.6:1:5.3. The highest occupied MO's of **8** are shown in Fig. 7. As in **2** the MO's are predicted to be linear combinations of the lone pairs of the P-CH_3 groups.

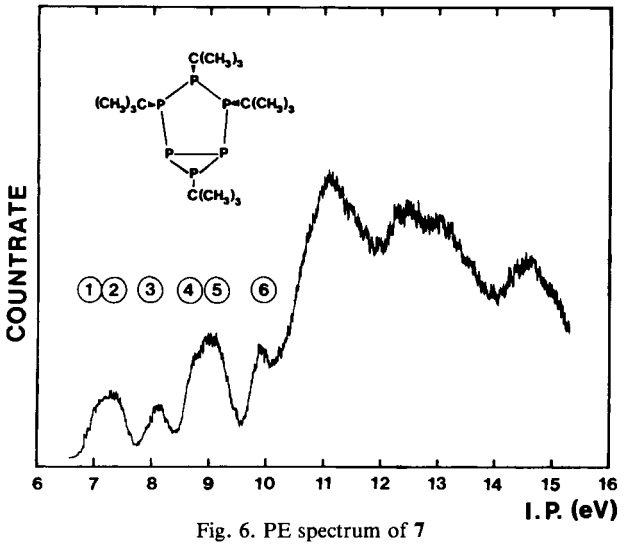

Fig. 6. PE spectrum of **7**

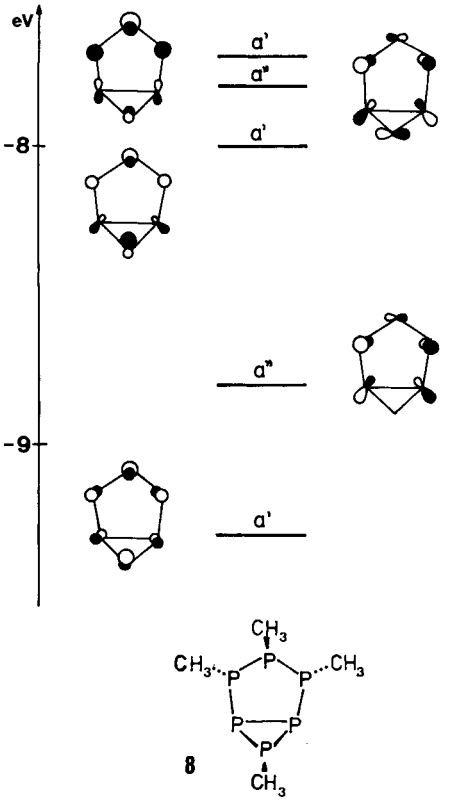

Fig. 7. Highest occupied MO's of **8** together with a schematic drawing of the wave functions

Table 3. Comparison between the measured vertical ionization potentials $I_{v,j}$ of **7** and calculated ones (MINDO/3, MNDO) for **8** assuming the validity of Koopmans' theorem (w = Walsh-type orbital)

Band	$I_{v,j}$	Assignment	$-\varepsilon_j$ (eV) MNDO	$-\varepsilon_j$ (eV) MINDO/3
①	7.1	n_P (ap), n_P (eq)	9.71(a′)	7.69(a′)
②	7.4	n_P (eq)	9.99(a″)	7.81(a″)
		n_P (b)	10.55(a′)	7.99(a′)
③	8.2	n_P (b)	11.54(a″)	8.82(a″)
④	8.9	n_P (ap), n_P (eq)	11.71(a′)	9.31(a′)
		w_1	12.18(a″)	9.60(a″)
		w_2	12.36(a′)	9.93(a′)
⑤	9.2	PC-σ	13.08(a″)	11.08(a″)
		PC-σ	13.26(a′)	11.39(a′)
⑥	10.0	PC-σ	13.42(a′)	11.63(a′)

Concluding Remarks

In connection with the present investigations on **1** and **2** it is interesting to consider the electronic structure of other phosphorus compounds known to possess a nortricyclane cage-type structure[15] like **6**[3], P_7^{3-} (**9**)[16,17], and P_4S_3 (**10**)[18]. The electronic structure of **9** has been investigated by MO calculations[11], that of **6** and **10** by model calculations and PE spectroscopic investigations[19–21]. In all compounds the same orbital sequence as predicted for **2** and shown in Fig. 2 and Table 1 is encountered. The highest occupied MO's can be looked at as linear combinations centered at the equatorial atoms followed by a lone pair centered at the apical P atom. These MO's are followed by orbitals localized mainly at the basal P_3 unit.

The main difference between **2** and **10** is the different energy of the occupied MO's and a sizeable difference between the basicity of the centers in **10** (the lone pair at the apical P atom is more basic than the lone pairs at the S atoms) while in **2** the basicity of the equatorial PCH_3 groups is very similar to the apical P atom. Thus in the case of **10** an attack of an electrophile at the apical center will yield the thermodynamically more favoured product, while in the case of **2** the kinetically and thermodynamically favoured substitution is predicted to take place at the steric most hindered position. These predictions are in line with findings that **10** forms complexes with transition metal carbonyls, e. g. $P_4S_3Mo(CO)_5$[22], while experiments to complex **6** have failed so far[5]. This lack of reactivity towards sterically ambitious electrophiles might be overcome by substituting the equatorial P atoms in the P_7 cage with more electronegative groups like CF_3 or CN. This should favour the attack of an electrophile at the apical P atom. According to our MNDO calculations on $P_7(SiH_3)_3$ (**11**) as model for **6** the orbital sequence is identical to that found for **2** and **10**. The main difference caused by the SiH_3 group can be seen by comparing the contour plots of some of the highest occupied MO's of **11** given in Fig. 8 with those of **2** shown in Fig. 3: The SiH_3 groups cause a stronger delocalization. As an example let us consider 9e. In **2** it is mainly localized at the equatorial P atoms while in **11** it is about equally distributed at the basal and equatorial P atoms.

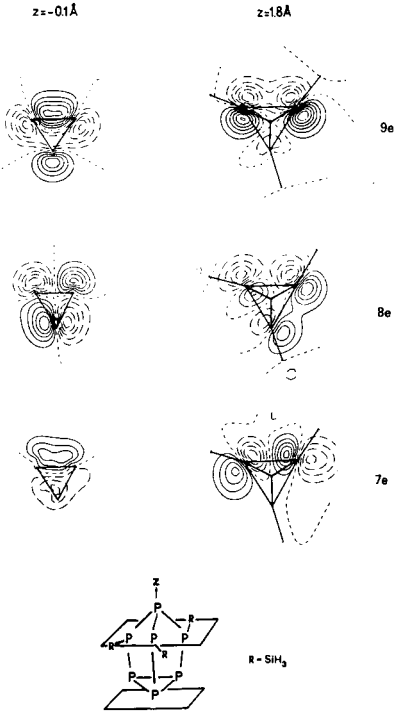

Fig. 8. Wave function contour diagrams of the highest occupied MO's of $P_7(SiH_3)_3$ (**11**)

We are grateful to the *Fonds der Chemischen Industrie* and the *BASF Aktiengesellschaft,* Ludwigshafen, for financial support. Thanks are due to *A. Flatow* for some PE measurements.

Experimental Part

The synthesis of compounds **1**[1], **2**[2], and **7**[14] has been described in the literature. The PE spectra of **1**, **2** and **7** were recorded on a PS 18 Spectrometer (Perkin Elmer Ltd., Beaconsfield, England) using a heated probe. The spectra were calibrated using Ar and Xe.

[1] *G. Fritz* and *R. Uhlmann,* Z. Anorg. Allg. Chem. **440**, 168 (1978).
[2] *M. Baudler, W. Faber,* and *J. Hahn,* Z. Anorg. Allg. Chem. **469**, 15 (1980).
[3] *W. Hönle* and *H. G. v. Schnering,* Z. Anorg. Allg. Chem. **440**, 171 (1978).
[4] *G. Fritz* and *R. Uhlmann,* Z. Anorg. Allg. Chem. **465**, 59 (1980).
[5] *G. Fritz* and *K. D. Hoppe,* unpublished results.
[6] *W. Hönle* and *H. G. von Schnering,* Z. Anorg. Allg. Chem. **465**, 72 (1980).
[7] *M. J. S. Dewar* and *W. Thiel,* J. Am. Chem. Soc. **99**, 4899 (1977).
[8] *R. C. Bingham, M. J. S. Dewar,* and *D. H. Lo,* J. Am. Chem. Soc. **97**, 1285 (1975). The calculations were carried out with MOPN Quantum Chem. Prog. Exch. **12**, 383 (1979)[9] using modified PC parameters[10].
[9] *P. Bischof,* J. Am. Chem. Soc. **98**, 6844 (1976).
[10] *G. Frenking, H. Götz,* and *F. Marschner,* J. Am. Chem. Soc. **100**, 5295 (1978).
[11] *M. C. Böhm* and *R. Gleiter,* Z. Naturforsch., Teil B **36**, 498 (1981).
[12] *R. Gleiter, M. C. Böhm,* and *M. Baudler,* Chem. Ber. **114**, 1004 (1981).
[13] *T. Koopmans,* Physica **1**, 104 (1934).

[14] *M. Baudler, Y. Aktalay, K.-F. Tebbe,* and *T. Heinlein,* Angew. Chem. **93**, 1020 (1981); Angew. Chem., Int. Ed. Engl. **20**, 967 (1981).
[15] *H. G. von Schnering,* in Homoaromatic Rings and Chains, *L. Rheingold* Edit., Elsevier Scientific Publishing Co., New York 1977; *H. G. von Schnering,* Angew. Chem. **93**, 44 (1981); Angew. Chem., Int. Ed. Engl. **20**, 33 (1981).
[16] *W. Dahlmann* and *H. G. von Schnering,* Naturwissenschaften **60**, 429 (1974); **59**, 420 (1973).
[17] *M. Baudler, H. Ternberger, W. Faber,* and *J. Hahn,* Z. Naturforsch., Teil B **34**, 1690 (1979); *M. Baudler, T. Pontzen, J. Hahn, H. Ternberger,* and *W. Faber,* ibid. **35**, 517 (1980).
[18] *Y. C. Leung, J. Wazer, S. van Houten, A. Vos, G. A. Wiegers,* and *E. H. Wiebenger,* Acta Crystallogr. **10**, 574 (1957).
[19] *J. D. Head, K. A. R. Mitchell, L. Noodleman,* and *N. L. Paddock,* Can. J. Chem. **55**, 669 (1977).
[20] *M. S. Banna, D. C. Frost, C. A. Mc Dowell,* and *G. Wallbank,* J. Chem. Phys. **66**, 3509 (1977); *P. H. Cannington* and *H. J. Whitfield,* J. Electron Spectrosc. Relat. Phenom. **10**, 35 (1977).
[21] *H. Bock, B. Soluki, G. Fritz,* and *W. Hölderich,* Z. Anorg. Allg. Chem. **458**, 53 (1979).
[22] *A. W. Cordes, R. D. Joyner, R. D. Shores,* and *E. D. Dill,* Inorg. Chem. **13**, 132 (1974).

[384/82]